

Searching for IR excesses in Sun-like stars observed by *WISE*

F. Cruz-Saenz de Miera*, M. Chavez, E. Bertone and O. Vega

Instituto Nacional de Astrofísica, Óptica y Electrónica, Luis Enrique Erro 1, Tonantzintla, Puebla, Mexico

Accepted . Received; in original form

ABSTRACT

We present the results of a search of infrared excess candidates in a comprehensive (29 000 stars) magnitude limited sample of dwarf stars, spanning the spectral range F2-K0, and brighter than $V=15$ mag. We searched the sample within the *WISE* all sky survey database for objects within 1 arcsecond of the coordinates provided by SIMBAD database and found over 9 000 sources detected in all *WISE* bands. This latter sample excludes objects that are flagged as extended sources and those images which are affected by various optical artifacts. For each detected object, we compared the observed $W4/W2$ ($22\mu\text{m}/4.6\mu\text{m}$) flux ratio with the expected photospheric value and identified 197 excess candidates at 3σ . For the vast majority of candidates, the results of this analysis represent the first reported evidence of an IR excess. Through the comparison with a simple black-body emission model, we derive estimates of the dust temperature, as well as of the dust fractional luminosities. For more than 80% of the sample this temperature is higher than 120 K, suggesting the presence of warm circumstellar dust. Complementary observations at longer wavelengths (far-IR and sub-mm) are required for better characterising and explaining the origin of this emission.

Key words: circumstellar matter – infrared: stars.

1 INTRODUCTION

An infrared excess (IR) around mature stars, measured as the flux in excess to that expected purely from the stellar photosphere, is produced by orbiting dust particles. This dust is destroyed by physical processes such as Poynting-Robertson drag, radiation pressure and photoevaporation in timescales much shorter than the stellar age and therefore, it must be replenished by collisions of planetesimals.

Since the unexpected discovery of an IR excess around Vega (α Lyrae, Aumann et al. 1984), infrared observations from space confirmed that the presence of circumstellar discs around main sequence (MS) stars is a common phenomenon (Trilling et al. 2008). However, these objects show a large distribution in dust temperature (T_{dust}) and mass and, while it is common to find cold debris discs ($T_{\text{dust}} < 120$ K), warm discs around this type of stars are indeed unusual and have been detected for a few stars (see, e. g., Kennedy & Wyatt 2012). In spite of their rarity, there are strong motivations for their study and they have posed interesting theoretical challenges to explain their presence and relatively large masses. On the one hand, warm material is expected to be close to the host star, within a few astronomical units, there-

fore, they represent valuable laboratories to study the potential correlation between the detected material and the presence of larger bodies (planets) in orbits similar to that of the Earth. On the other hand, their fractional luminosities, well above the estimated fractional luminosity of the solar system zodiacal dust cloud (Dermott et al. 2002), escape explanations through the models of terrestrial planet formation (Kenyon & Bromley 2005) or the steady state planetesimal grinding, and have to be formed through other mechanisms such as transient events (Wyatt et al. 2007). Two main approaches have been suggested to explain the origin of hot dust: one of them considers a temporary increment in collisions due to dynamical instabilities, causing a so-called late heavy bombardment. Such a scenario has been proposed by Lisse et al. (2012) to account for the debris disc around η Corvi. The second mechanism is the catastrophic collision of two rocky, planetary-scale bodies, which could explain the debris disc around BD+20 307 (Weinberger et al. 2011). Therefore, the study of warm debris discs not only is important to understand the dynamical evolution and the presence of small bodies in planetary systems, but also to understand the formation of terrestrial planets and the history of our solar system.

In this context, the recent Wide-field Infrared Survey Explorer (*WISE*) mission (Wright et al. 2010) is certainly providing a fresher benchmark for characterising warm cir-

* E-mail: fsaenz@inaoep.mx (FCSM); mchavez@inaoep.mx (MC); ebertone@inaoep.mx (EB), ovega@inaoep.mx (OV)

cumstellar material around main sequence stars. *WISE* has conducted an all sky survey with an unprecedented sensitivity (orders of magnitude better than its early predecessor *IRAS*) in four bands: 3.4, 4.6, 12, and 22 μm , denoted as W1, W2, W3, and W4, respectively. *WISE* data, together with the outcomes from *AKARI* (see, e.g., Fujiwara et al. 2009, 2013), represent valuable means for demographic studies of warm circumstellar material. To date, most stellar analyses involving *WISE* data had focused on stellar samples aimed at searching for IR excesses in stars observed by the *Kepler* mission, including stars that are known to host transiting planetary companions (Krivov et al. 2011; Lawler & Gladman 2012; Ribas et al. 2012; Kennedy & Wyatt 2012), and identifying possible correlations of mid-IR excesses and rotation (Mizusawa et al. 2012).

In this paper we present a study of the *WISE* data base with the goal of searching excesses at 22 μm within a comprehensive magnitude-limited sample of Sun-like stars. The resulting set of excess candidates and the parameters derived for the circumstellar material will serve as a basis for future studies at longer wavelengths, which may shed light on the frequency and properties of warm circumstellar discs around this kind of stars.

2 THE STELLAR SAMPLE AND *WISE* DATA

The sample was constructed through a selection process that started by querying the SIMBAD database for main sequence stars. We imposed a limiting magnitude of $V=15$ mag, luminosity class V, and spectral types between F2 and K0. We also required 2MASS data to be available. From this first selection we got the information of nearly 29 000 stars. It is important to note that the query by criteria in SIMBAD results in a wide variety of stellar sources with the vast majority (90%) corresponding to objects whose object type is *only* an asterisk (*), this is, stars which do not present or has not been identified any peculiarity (binarity, variability, etc.). The other most prominent stellar groups within this sample are stars in binary or multiple systems (5%), pre-main sequence objects (2%), stars in clusters and associations (2%), and the remaining corresponding to a wide variety of stellar sources, mainly variable stars of different types.

WISE is a NASA funded explorer mission that was launched at the end of 2009 and conducted an all sky survey in four IR bands, with an angular resolution of 6.1, 6.4, 6.5, and 12.0 arcsec for W1, W2, W3, and W4, respectively. In spite of having slightly more than a third of the collecting area of its most immediate predecessor *AKARI*, its high performance detectors (with 4 million pixels) pushed down the limiting flux density to about 6 mJy at 22 μm , which is nearly 20 times better than that of *AKARI* at 18 μm (Ishihara et al. 2010; Wright et al. 2010). The *WISE* all sky data release¹ contains information of more than 500 million objects, half of which are expected to be stellar sources, with an astrometric accuracy of better than 0.5 arcsec even

for faint sources. The enhanced *WISE* sensitivity has provided and will provide in years to come access to a number of previously unidentified mid-IR excesses around solar-like stars.

We used the stellar coordinates to identify *WISE* counter parts. The constraints we imposed for the selection were *WISE* sources to be located within one arcsecond in radius and that reported fluxes at all *WISE* bands have signal-to-noise ratios (SNR) larger than 5. Additionally, following the criteria described in Lawler & Gladman (2012), we have also excluded objects whose *WISE* data, in one or more bands, appear flagged as having contamination of halos, diffraction spikes, and optical ghosts due to nearby bright sources, as well as those flagged as extended sources. We have also excluded objects that are labelled as saturated in any of the W2, W3, and W4 bands, i.e. some of our objects after this selection might be saturated in the W1 band. After this process the sample was reduced to about 9 500 detected objects.

Even though we do not expect interstellar extinction to be important for many objects in this later set, we have applied an extinction correction at the J, K_S and W2 bands to those objects for which we identified reddening in excess of $E(B-V)=0.05$ mag. Reddening has been estimated from the comparison of the B-V color available in SIMBAD and the color index–spectral type calibration of Pecaut, Mamajek & Bubar (2012). The extinction curve used for this procedure was that of Rieke & Lebofsky (1985). For the W4 band no extinction correction was applied, since at this wavelength the interstellar reddening is expected to have negligible effects.

Detections are presented in Fig. 1, where we plot the *WISE* flux ratio W4/W2 versus the 2MASS flux ratio J/K_S , for the entire sample. As a reference we have overplotted (connected stars) the theoretical photospheric line constructed from NEXTGEN model fluxes (Hauschildt et al. 1999) in the effective temperature (T_{eff}) range 4 000–7 000 K with the step available in the model flux library of 200 K. All theoretical fluxes are of solar chemical composition and surface gravity $\log g=4.5$ dex. Note that most data points clearly cluster around the photospheric line, and that point clustering extends well beyond these effective temperature limits, particularly at the lower temperature edge. This extension is most probably due to the low temperature ($T_{\text{eff}} < 5 000$ K) members of binaries and multiple systems, both identified or probably still unidentified, and to reddened objects. Note also that numerous objects in Fig. 1 are located well away from the photospheric line, hence plausibly corresponding to objects with prominent excesses.

3 FINDING IR EXCESS CANDIDATES

In order to determine if there is an excess and its quantification, we measured the difference between the observed flux ratios W4/W2 and theoretical photospheric predictions for a given J/K_S and compared with the corresponding error σ_{tot} . Errors in our data points have been calculated by considering three different sources: photometric errors σ_{obs} , calibration uncertainties σ_{cal} , and errors associated with the photospheric parameters σ_{phot} . The σ_{obs} was obtained from the quoted uncertainties available within the *WISE* data release

¹ <http://wise2.ipac.caltech.edu/docs/release/allsky/>

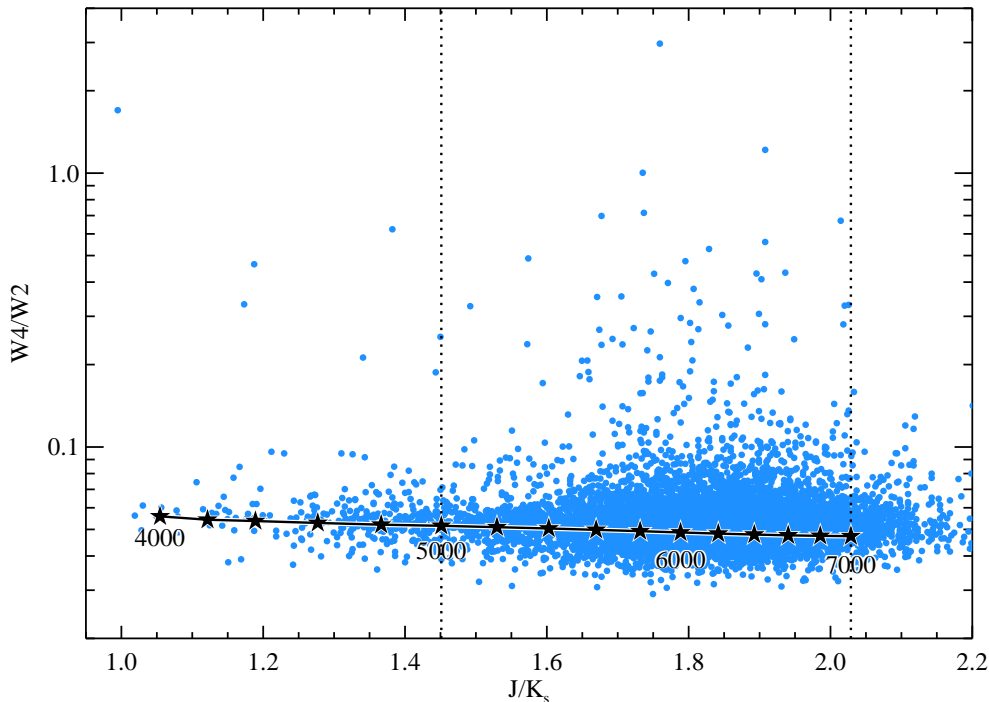


Figure 1. Flux ratios diagram using *WISE* data at the W2 and W4 bands and the 2MASS fluxes at J and K_S . Blue dots represent the detected stars classified as main sequence and brighter than $V=15$ mag in SIMBAD database. The black stars indicate the position of the photospheric flux ratios calculated from theoretical fluxes extracted from the NEXTGEN library (Hauschildt et al. 1999). The vertical dashed lines indicate the approximate temperature boundaries for K0 (5 000 K) and F2-type (7 000 K) stars.

for each band. Absolute calibration uncertainties of *WISE* are estimated to be 2.4, 2.8, 4.5 and 5.7% for the W1, W2, W3 and W4, respectively (Jarrett et al. 2011). For σ_{phot} we considered the effects of varying surface gravity ($3.5 \leq \log g \leq 5.0$) and metallicity ($-3.5 \leq [M/H] \leq 0.0$), once an effective temperature is assigned to each star by matching its J/K_S color with the NEXTGEN theoretical fluxes. The total error budget is then $\sigma_{\text{tot}} = \sqrt{\sigma_{\text{phot}}^2 + \sigma_{\text{obs}}^2 + \sigma_{\text{cal}}^2}$. For the vast majority of the detected objects σ_{obs} is the dominant source of uncertainty.

We have considered an excess whenever $(W4/W2_{\text{WISE}} - W4/W2_{\text{phot}})/\sigma_{\text{tot}} \geq 3$, where $W4/W2_{\text{WISE}}$ is the extinction corrected observed color, and $W4/W2_{\text{phot}}$ is the theoretical photospheric flux ratio calculated using the appropriate transmission functions and color corrections (Wright et al. 2010). Through this analysis we obtained a total of 313 excess candidates. At this stage it is necessary to elaborate in some cautionary notes on the reliability of these excesses.

4 WISE IMAGES EXAMINATION AND FINAL LIST OF EXCESS CANDIDATES

As a first step to assess on the quality of the excess candidates, we have carefully visually inspected images at the four bands for each of the 313 objects. Figure 2 summarises the results of this examination. We found numerous spurious detections in which no object is evident in the W4 band. An example of this situation is illustrated in the top two panels

of the figure for the star HD 78710. The object is clearly present in W2 (left) and absent in W4 (right). This effect is a product of the source extraction in the *WISE* pipeline processing and the complex backgrounds that characterise W4 images. In the second row of panels we show another case, exemplified by the star V900 Per, in which infrared emission at $22 \mu\text{m}$ is detected, but cannot be associated with a point source. In the third row we display the case of HD 227748 where there is an offset in the position of the source identified in W2 with respect to that in W4, and, in any case, the faint source cannot be unambiguously distinguished from emission peaks of the interstellar medium.

Objects in the above described cases (116 stars) were rejected leaving the final sample with 197 objects. In the panels at the bottom of Fig. 2 we illustrate an excess detection case for HD 107899. The star is clearly visible in the W4 band, even if it appears located within a region with diffuse emission. However, many detections correspond to well isolated point sources.

In Fig. 3 we illustrate the distribution of sources with excesses at W4. The y-axis gives the flux ratios $(W4/W2)_N$ normalised to the expected photospheric values versus J/K_S . The largest excess corresponds to the F5V type HD 39415, which is the only *IRAS* source in our set of excess candidates. This object was not detected at 60 and $100 \mu\text{m}$ and its flux at $25 \mu\text{m}$ was labeled as of moderate quality. Note that in the determination of excesses we have implicitly considered that the 2MASS fluxes and the flux at W2 are purely photospheric, as assumed in the analysis of Krivov et al. (2011).

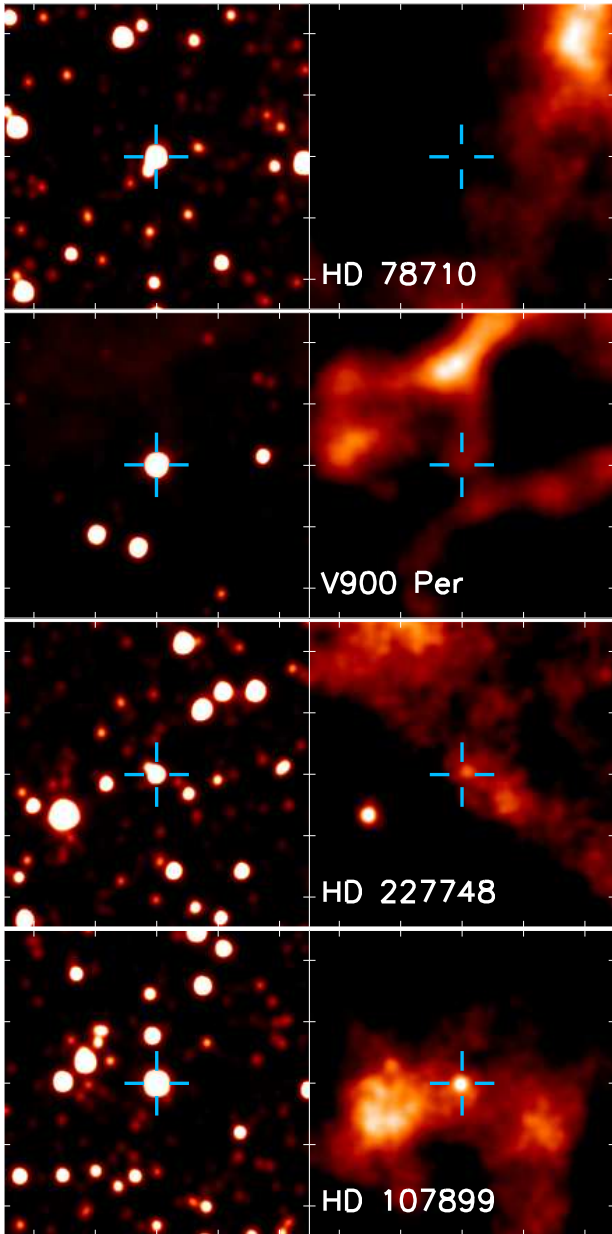


Figure 2. WISE W2 (left panels) and W4 (right panels) 5×5 arcmin images of HD 78710, V900 Per, HD 227748, and HD 107899; north is up and east is left. The color scale spans from 0 to 20 times the standard deviation of the background for W2, while for W4 the interval is reduced to 0– 3σ . The three upper panels show objects that we classified as non-detections in W4, while HD 107899 is included in our catalog.

Nevertheless, this assumption might not be correct for the few young stellar objects included in the sample. The object-type statistics for the 3σ sample closely resembles that of the original sample from SIMBAD: isolated field stars account for the majority (about 90%), while the remaining objects belong to various stellar types (stars in double systems, pre-main sequence stars, etc.).

In left panel of Fig. 4 we present the spectral type distribution of the excess candidates, which is clearly dominated by the F-type stars, while in the right panel of that figure

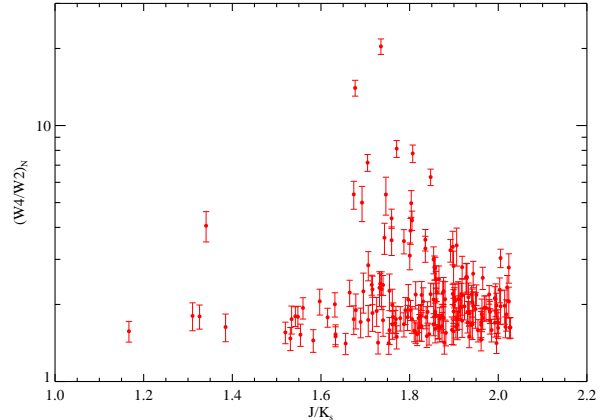


Figure 3. Normalised flux ratios $(W4/W2)_N$ for the fiducial set of objects with excesses at 3σ .

we show distance distribution for 68 objects with available *Hipparcos*' data. In this group, most of the 3σ excesses are found in objects closer than 300 pc. There are, however, four objects farther away. Note the absence of the nearest stars (with distances less than 47 pc) in the histogram. The reason for this is explained by the adopted selection requirements for searching within the *WISE* database, as nearer objects are sources flagged as extended, saturated, and/or affected by one or more of the above mentioned optical artifacts in the W2 band.

5 DISCUSSION AND CONCLUSIONS

We have identified a sample of 197 main-sequence objects that display 3σ IR excesses, many of which are present at both W3 and W4 *WISE* bands. This number corresponds to about 2% of the parent sample of *WISE* detections. In our resulting sample of IR excesses, 20 have previously reported observations in the mid-IR. The majority of these objects belong to the Scorpius-Centaurus association and have been studied with *Spitzer* (Chen et al. 2011) and *WISE* (Rizzuto, Ireland, & Zucker 2012). There are also some Pleiades members, one of which is HD 23514, amongst the dustiest systems in this cluster (Rhee et al. 2008; Sierchio et al. 2010). In the particular case of *WISE* data, Krivov et al. (2011) report an excess of one target, TrES-2, that fulfills our selection criteria. However, this object has not been included in our analysis because the SNR in the W4 band is below our adopted value of 5.

In Fig. 5 we display the spectral energy distributions of four stars in our sample of excess candidates. Data points in red correspond to the fluxes of both 2MASS and *WISE* bands. The theoretical fluxes for each star have been calculated by interpolating within the NEXTGEN grid for the effective temperatures derived from their J/K_S ratios. The solid line in each panel represents the star+disc spectral energy distribution (SED). This integrated SED was obtained following three steps. First, the theoretical fluxes were scaled in J to match the observational data points. Second, we created an extensive grid of black body flux densities for temperatures (T_{disc}) in the range 20–500 K (at a step of 1 K),

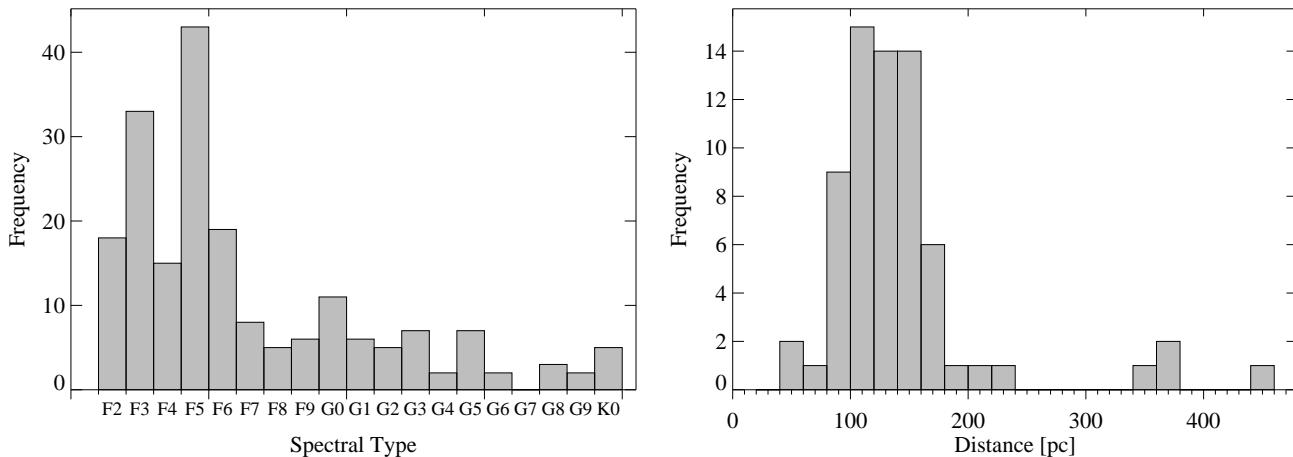


Figure 4. On the left we show the spectral type distribution of the 197 objects that display IR excesses. The distance distribution for the 68 objects with available Hipparcos parallaxes is shown on the right. In the distance histogram the bins are of 20 pc.

and fractional luminosities (F_{disc}) (Wyatt 2008), in the interval 10^{-1} - 10^{-5} . Third, we conducted a χ^2 minimization that provided the combination of T_{disc} and F_{disc} that best fit *WISE* bands. The best fit values are indicated in each panel of Fig. 5.

In Table 1, we list some of the sample stars for which we identified a prominent IR excess. The table provides the stellar identification, the full set of object types available in SIMBAD, the V magnitude and spectral types as given in SIMBAD, the stellar effective temperature and its uncertainty derived from the quoted errors in the J and K_S , the normalised flux ratios $W3/W2_N$ and $W4/W2_N$ associated with the SNRs at the W3 and W4 bands. In the last two columns, we report the estimates for the dust temperature and fractional luminosities and their uncertainties, that were obtained fitting the *WISE* fluxes $\pm \sigma_{\text{tot}}$. A label after the identification indicates those objects included in previous IR observational programs. The table with the full stellar sample is available in electronic form.

In Fig. 6 we plot the distribution of the black body temperature associated to the 197 disc candidates of our sample. The majority of the stars (161 out of 197) have warm circumstellar material with $T_{\text{disc}} > 120$ K, with a peak around 180 K; this result was expected because of the wavelength range covered by the *WISE* observations. About 46% (90) of the stars also show 3σ excesses in W3 indicated with the shaded area in the figure. Note that this later subsample clearly occupies the hotter end of the distribution. In these cases we have at least two non-photospheric points available to determine the black body properties, hence the fitting procedure provides better estimates of the disc parameters. In general, the relative errors of both T_{disc} and F_{disc} in objects with W3 and W4 excesses are lower than in objects displaying an excess in only W4. In contrast, the distribution of fractional luminosities (see Fig. 7) does not indicate any particular trend for stars displaying also a W3 excess. The vast majority of excess stars present a disc fractional luminosity in the interval 10^{-3} - 10^{-4} . However, ten sources have a very strong IR excess, with $F_{\text{disc}} > 10^{-2}$, and nine of them appear to have a very low temperature estimate ($T_{\text{disc}} \leq 69$ K). The star YZ Cep, also has a large frac-

tional luminosity, and exhibits the hottest disc of our sample ($T_{\text{disc}} = 442$ K; see Fig. 5). YZ Cep is an irregular variable of RW Aurigae type (Ross 1926) and it is classified as a T Tauri star (Kardopolov et al. 1987). Another object that presents a hot disc is HD 23514. Our modelling provides a dust temperature of 405 K which is significantly lower than 750 K obtained by Rhee et al. (2008). This difference is most probably due to the fact that we conducted the fit at longer wavelengths (W3, W4), while (Rhee et al. 2008) fit the data up to $\lambda = 12 \mu\text{m}$.

In the analysis here presented, we have examined *WISE* images to identify false detections. Such scrutiny turned out to be of fundamental importance since, as we have demonstrated, nominal high quality fluxes in the *WISE* database do not always correspond to a detected source. The lack of this double-check process yielded contrasting results in searches for IR excesses in stars of the *Kepler* field (Ribas et al. 2012). To further check on the reliability of our reported excesses we have compared *WISE*-W4 fluxes with those collected with *Spitzer*-MIPS at $24 \mu\text{m}$. In Fig. 8 we plot this comparison for three different stellar sets. Squares in green correspond to the stars in our sample with previously reported IR data. Dots in blue are the fluxes reported in Eiroa et al. (2013) for the bright stars included in the Herschel-DUNES program (Eiroa et al. 2010). The red triangles indicate the position of stars in Chen et al. (2011). For this latter set we have extracted *WISE* data considering the same criteria as for our working sample. It is interesting to see that there is a remarkable consistency down to the weakest source in our sample (3.8 mJy for TYC 9139-2239-1), whose flux level is indicated with the horizontal dotted line.

A mid-IR excess indicates, in general, the existence of warm circumstellar material. Apart from the few very hot objects, at these wavelengths we are mapping the Wien-edge of the energy distributions, therefore, the lack of an excess does not necessarily imply the absence of circumstellar material. Cool discs ($T_{\text{dust}} < 50$ K) have their imprints at longer wavelengths, and very little or no excess in the mid-IR. The results of this work incorporate numerous newly identified objects with mid-IR excesses and will certainly motivate new

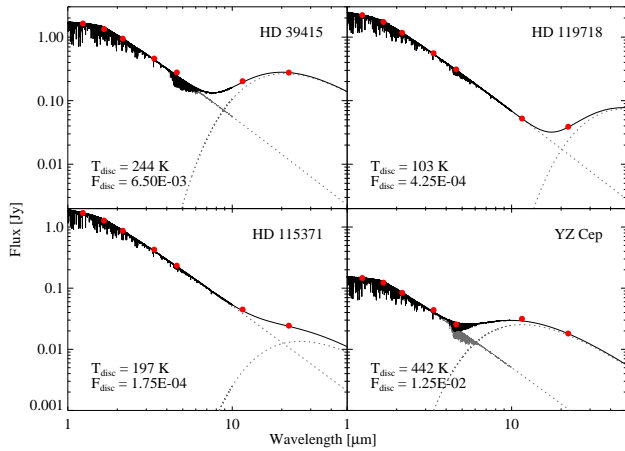


Figure 5. Spectral energy distributions of four stars that display prominent $22\mu\text{m}$ excesses. Observational data points (red dots) mark the J, H, and K_S 2MASS magnitudes, extracted from SIMBAD, and four *WISE* bands. The continuous lines correspond to the best fit of the stellar photosphere plus a black body. In each panel we indicate the black body temperature and fractional luminosity that delivers the best fit.

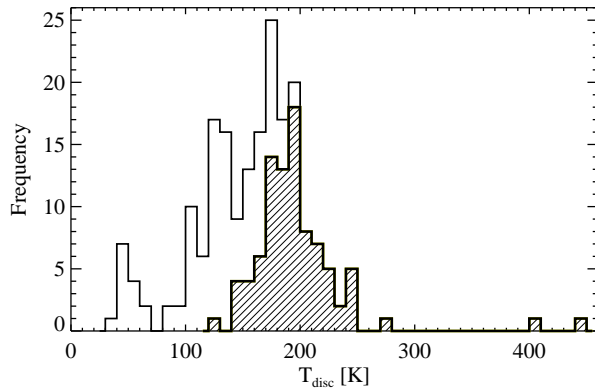


Figure 6. Distribution of the black body temperature of the disc candidates of our sample. The shaded area indicates the distribution of those objects that also display a 3σ excess in W3.

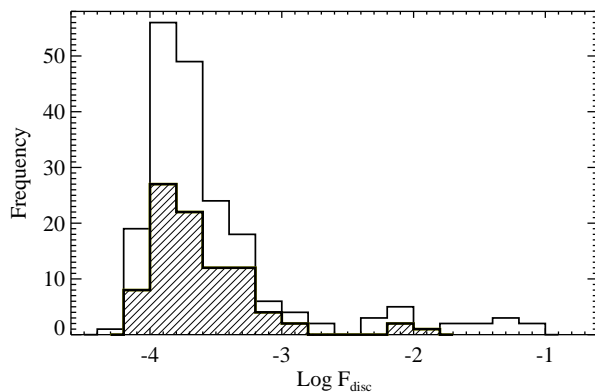


Figure 7. Distribution of the fractional luminosity of the disc candidates of our sample. The shaded area indicates the distribution of those objects that also display a 3σ excess in W3.

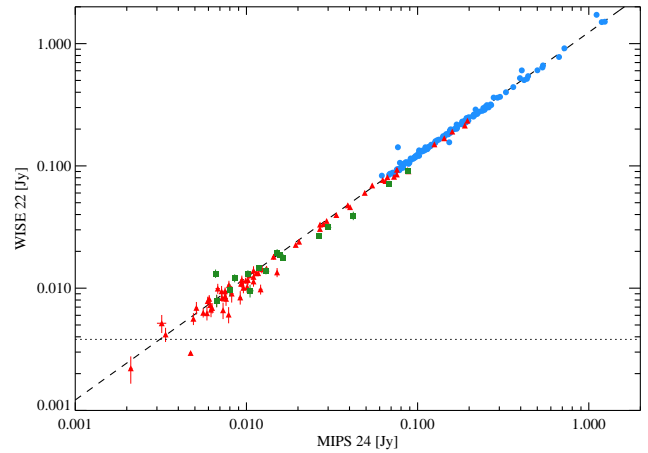


Figure 8. Comparison between *WISE*-W4 and *Spitzer*-MIPS at $24\mu\text{m}$. Blue circles and red triangles are sources from Eiroa et al. (2013) and Chen et al. (2011), respectively. Data from Chen et al. (2011) consist of the 65 stars in their sample that accomplished the *WISE* quality selection criteria adopted in this work. Green squares are the excess candidates included in the present work. Error bars are smaller than the symbol size for most stars. The agreement of the two instruments is evident down to the lowest W4 flux level in our sample of excess candidates indicated with the dotted line.

observational programs at far-IR, sub-mm and mm that are required to better characterise the material around Sun-like stars.

ACKNOWLEDGMENTS

We thank the anonymous referee for constructive comments that improved the presentation of this work. MC and FCSM would like to thank CONACyT for financial support through grant number 134985. This publication makes use of data products from the Wide-field Infrared Survey Explorer, which is a joint project of the University of California, Los Angeles, and the Jet Propulsion Laboratory/California Institute of Technology, funded by the National Aeronautics and Space Administration. This research has made use of the SIMBAD database, operated at CDS, Strasbourg, France.

REFERENCES

- Aumann H. H., Beichmann C. A., Gillett F. C., de Jong, T. Houck, J. R. et al., 1984, *ApJL*, 278, L23
 Chen C. H., Mamajek E., Bitner M. A., Pecaut M., Su K. Y. L., et al., 2011, *ApJ*, 738, 122
 Dermott S. F., Durda D. D., Grogan K., Kehoe, T. J. J. 2002, in *Asteroids III*, ed. W. F. Bottke Jr. et al. (Tucson, Univ. Arizona Press), 423
 Eiroa C., Fedele D., Maldonado J., González-García B. M., Rodmann J., et al., 2010, *A&A*, 518, L131
 Eiroa C., Marshall, J. P., Mora, A., Montesinos B., Absil, O., et al. 2013, *A&A*, 555, 11
 Fujiwara H., Ishihara D., Kataza H., Onaka T., Yamashita T. et al., 2009, in proceedings of the conference *AKARI*,

Table 1. Subsample of stars with prominent mid-IR excesses.

star ID	O-types	V	Sp. Type	T_{eff} (K)	$\frac{W3}{W2_N}$	SNR _{W3}	$\frac{W4}{W2_N}$	SNR _{W4}	T_{disc} (K)	F_{disc}
HD 15053	*,IR	9.50	F7V	6610±250	1.29	2.11	1.67	3.95	166 ⁺⁴² ₋₃₀	9.25E-05 ^{+3.25E-05} _{-1.75E-05}
HD 23380	*,IR	8.38	F2V	6870±330	1.28	3.10	1.61	8.19	183 ⁺²⁶ ₋₂₄	7.50E-05 ^{+7.50E-06} _{-5.00E-06}
HD 39415 [†]	*,IR	8.40	F5V	5810±370	5.18	50.05	20.37	45.18	244 ⁺¹ ₋₄	6.50E-03 ^{+0.00E+00} _{-2.50E-04}
HD 65516	*,IR	8.91	F5V	6210±210	1.31	3.68	1.53	7.00	205 ⁺³⁶ ₋₂₇	1.00E-04 ^{+0.00E+00} _{-0.00E+00}
HD 115371	*,V*,IR	8.29	F3V	6600±290	1.41	7.35	2.19	13.22	197 ⁺¹⁶ ₋₁₅	1.75E-04 ^{+0.00E+00} _{-0.00E+00}
HD 119718 [†]	*,IR	8.03	F5V	6440±250	1.23	0.26	2.65	7.75	103 ⁺⁴⁴ ₋₅₉	4.25E-04 ^{+6.46E-02} _{-2.00E-04}
HD 125344	*,IR	9.78	F7V	6180±240	1.25	0.88	3.58	10.64	105 ⁺¹⁸ ₋₅₂	7.25E-04 ^{+1.93E-02} _{-2.25E-04}
HD 141227	*,IR	8.85	F5V	5710±170	1.73	14.63	7.16	24.76	164 ⁺⁶ ₋₂	1.50E-03 ^{+0.00E+00} _{-0.00E+00}
HD 158815	*,IR	9.70	G1V	5900±300	1.51	7.08	4.33	14.21	163 ⁺⁹ ₋₁₀	7.50E-04 ^{+7.50E-05} _{-5.00E-05}
HD 196813	*,IR	9.72	G3V	5990±280	1.41	4.30	3.53	8.48	147 ⁺¹⁵ ₋₁₂	5.75E-04 ^{+1.00E-04} _{-7.50E-05}
HD 204765	*,pr*,IR	9.91	G1V	6040±210	1.31	2.15	3.10	6.88	133 ⁺²⁴ ₋₁₆	4.50E-04 ^{+1.50E-04} _{-1.00E-04}
YZ Cep	*,V*,RI*,IR	11.40	G0V	5820±180	8.77	62.90	14.54	17.98	442 ⁺⁵⁸ ₋₅	1.25E-02 ^{+0.00E+00} _{-2.50E-03}

[†] Star with previous mid-IR observations

a Light to Illuminate the Misty Universe, Ed. Takashi Onaka, Glenn J. White, Takao Nakagawa, and Issei Yamamura, ASP Conference Series, 418, 109

Fujiwara H., Ishihara D., Onaka T., Takita S., Kataza H. et al., 2013, A&A, 550, 45

Hauschildt P., Allard F., Baron E., 1999, ApJ, 512, 377

Ishihara D., et al., 2010, A&A, 514, A1

Jarrett T. H., Cohen M., Masci F., et al., 2011, ApJ, 735, 112

Kardopolov V. I., Filip'ev G. K., Shajmieva A. F., Shute-mova, N. A. 1987, Peremennye Zvezdy, 22, 461

Kennedy G. M., Wyatt M. C., 2012, MNRAS, 429, 91

Kenyon S. J., Bromley B. C. 2005, AJ, 130, 269

Krivov A. V., Reidemeister M., Fiedler S., Lohne T., Neuhauser R., 2011, MNRAS, 418, L15

Lawler S. M., Gladman B., 2012, ApJ, 752, 53

Lisse C. M., Wyatt M. C., Chen C. H., Morlok A. et al., 2012, ApJ, 747, 93

Mizusawa T. R., Rebull L. M., Stauffer J. R., Bryden G., Meyer M. et al., 2012, AJ, 144, 135

Pecaut M., Mamajek E., Bubar E. J., 2012, ApJ, 746, 154

Rhee J. H., Song I., Zuckerman B. 2008, ApJ, 675, 777

Ribas A., Merin B., Ardila D. R., Bouy R. H., 2012, A&A, 514, 38

Rieke G. H., Lebofsky M. J., 1985, ApJ, 288, 618

Rizzuto A. C., Ireland M. J., Zucker D. B., 2012, MNRAS, 421, L97

Ross F. E. 1926, AJ, 36, 122

Sierchio J. M., Rieke G. H., Su K. Y. L., Stauffer J. R., Gorlova N. I., 2010, ApJ, 712, 1421

Trilling D. E., Bryden G., Beichman C. A. et al., 2008, ApJ, 674, 1086

Weinberger A. J., Becklin E. E., Song I., Zuckerman, B., 2011, ApJ, 726, 72

Wright E. L., Eisenhardt P. R. M., Mainzer A. K., Ressler M. E., Cutri Roc M. et al., 2010, AJ, 140, 1868

Wyatt M. 2008, ARA&A, 46, 339

Wyatt M. C., Smith R., Greaves J. S. et al. 2007, ApJ, 658, 569

This paper has been typeset from a \LaTeX file prepared by the author.